Springer

KSME

Journal of Mechanical Science and Technology 33 (7) (2019) 3257~3263
www.springerlink.com/content/1738-494x(Print)/1976-3824(Online)
DOI 10.1007/s12206-019-0621-6

Viscous heating and temperature profiles of liquid water flows in copper nanochannel †

Quyen Van Dinh[1], Truong Quoc Vo[2] and BoHung Kim[3,*]

[1]*School of Mechanical and Materials Engineering, Washington State University, Pullman, WA 99164-2920, United States*
[2]*Laboratory of Engineering Thermodynamics (LTD), Technical University of Kaiserslautern, Erwin-Schrodinger-Str. 44, Kaiserslautern 67663, Germany*
[3]*School of Mechanical Engineering, University of Ulsan, Ulsan 680-749, Korea*

(Manuscript Received September 15, 2018; Revised March 18, 2019; Accepted March 27, 2019)

Abstract

Understanding nanoscale fluidic transport becomes increasingly important due to the rapid development of nanotechnology and nanofabrication. By using molecular dynamics (MD) simulations, we investigated the viscous heating of water flows in copper nanochannels. The two scenarios that were studied are Couette flows and Poiseuille flows. We observed the scale effects on the distribution of fluid density, streaming velocity, fluid viscosity, and temperature across the channel. The results revealed the significant effects of surface forces on causing a large deviation between simulation results and classical hypothesis. We found that the energy equation coupled with the thermal-slip boundary conditions still fails to predict the temperature distributions. Hereby, further scale effects are taken into account, which leads to better predictions. The model that we developed in this study shows the relative deviation to the simulation data within 5 %, which is small compared to the conventional continuum approach (i.e., up to 51 %).

Keywords: Molecular dynamics (MD); Nanoscale fluid flow; Thermal-slip boundary condition; Navier-Stokes-type prediction; Viscous heating

1. Introduction

Nano-fluidics plays an important role in nanosystems and nanodevices [1, 2], leading to the necessity of understanding its momentum and energy transport phenomena. Viscous heating in nanochannels has been an interesting topic due to its sub-continuum scale-effect on momentum and energy behaviors of nanoconfined flow [3-6]. Those studies found that when the continuum description is incorporated with the interface effects and modified boundary conditions, the so-called continuum-based modified-analytical solutions, they can adequately predict nanoscale fluid transport phenomena. In addition to viscous heating, we considered further effects at small scale such as thermal conductivity, and density, which usually differ from the bulk values. To pursue the procedure, we used non-equilibrium three-dimensional MD simulations to proceed with our numerical experiments.

This study is organized as follows: In Sec. 2, we describe the MD three-dimensional model and non-equilibrium simulation to study the flow behavior, such as density, temperature, and velocity. Next, we use modified-thermal-slip boundary conditions coupled with the continuum energy equation to predict the temperature profile of water [5]. In Sec. 3, we discuss the results, focusing on temperature prediction and discuss how well the solution of Navier-Stokes equation is modified to fit the fluid behavior at the nanoscale. That is the unveiled backlog from previous research about nano-scale fluid flows [5-7]. In the final section, our distinguished finding is that the utilizing of temperature jump boundary conditions with the impact of interfacial viscosity as well as the thermal conductivity correction can scientifically establish a highly consistent temperature prediction for nanofluid flow.

2. Simulation model and theoretical background

Fig. 1 shows a schematic of velocity and temperature profile for (a) shear-driven, (b) force-driven flow and (c) MD simulation model of water confined between two parallel copper-plates. We initially set the simulation with NVT (constant number of molecules, constant volume, and constant temperature) ensemble to establish system equilibrium. In this state, the Maxwell–Boltzmann velocity distribution is used as the initial velocity for all molecules, and Nosé–Hoover thermostat-maintained system temperature of 300 K. We applied heat baths to the walls as shown in Fig. 1(c). The method has been widely used [7-12]. The shear-driven and force-driven

*Corresponding author. Tel.: +82 52 259 2705, Fax.: +82 52 259 1680
E-mail address: bohungk@ulsan.ac.kr
† Recommended by Associate Editor Seongwon Kang

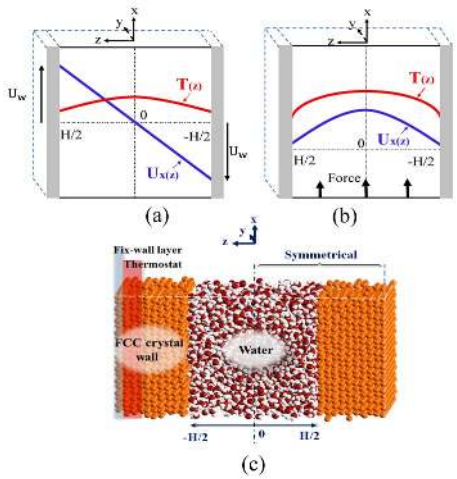

Fig. 1. Schematic of velocity and temperature profile for (a) shear-driven; (b) force driven flow through a representative cell; (c) MD simulation model of water confined between two parallel copper-plates.

flows are enabled by setting the wall a velocity of 50 nm/ns and by setting gravity of 49 m/s^2. We performed simulations for 50 ns: 2 ns to reach an isothermal steady state, 8 ns to ensure that the system attains steady state in presence of the heat flux, and two periods of 20 ns for a production run and statistical averaging. The time step is 1.0 fs. All simulations were performed using LAMMPS [8]. We used the many-body potential embedded (EAM) for the wall. The long-range electrostatic force is calculated by particle-particle, particle-mesh (PPPM) solver and the density of liquid water for all cases studied is maintained at 0.997 kg/m^3. We used the truncated LJ (12–6) potential for the van der Waals interactions between molecules:

$$E\left(r_{ij}\right)=\left[\left(A/r_{ij}^{12}-B/r_{ij}^{6}\right)-\left(A/r_{c}^{12}-B/r_{c}^{6}\right)\right], \quad (1)$$

where $A = 4\varepsilon\sigma^{12}$, $B = 4\varepsilon\sigma^{6}$, ε is the binding potential between atoms, r_{ij} is the intermolecular distance, σ is the molecular distance, and r_c is the cut-off distance.

A water molecule is a simple point charge-exchange (SPC/E) model [13]. We measured the local temperature in each slab bin using the average atomic kinetic energies.

$$T=(\frac{1}{3}N_n k_B)\sum_{i=1}^{N_n} m_i V_i^2 , \quad (2)$$

where k_B is the Boltzmann constant, N_n is the number of atoms in a slab bin, and m_i and V_i are mass and velocity of the i^{th} atom in the layer, respectively. The calculation of stress tensor components includes the kinetic and vial terms where the bin-wise streaming velocity is subtracted prior to the calculation [14, 15].

The dynamic viscosity (η) of the water is calculated as the ratio of the shear stress δ_{xz} component over the applied shear rate $\dot{\gamma}$:

$$\eta=-<\delta_{xz}>/\dot{\gamma}=\left(S_{xz}N/\Omega\right)/\dot{\gamma} , \quad (3)$$

where S_{xz} is per atom xz- shear stress tensor, N is the number of atoms, and Ω is the volume of one specified slab bin. The Navier-Stokes equation reads:

$$\rho\left(D\vec{V}/Dt\right)=-\nabla p+\rho\vec{g}+\eta\nabla^2\vec{V} , \quad (4)$$

with ρ is water density, p is pressure and g is an external force field. The continuum energy equation for the shear-driven flow is:

$$-d^2T/dz^2=\eta(\dot{\gamma}^2)/k , \quad (5)$$

where k is thermal conductivity. The temperature profile T(z) is:

$$T(z)=-(\alpha/2)z^2+c_1 z+c_2 , \quad (6)$$

where c_1 and c_2 are constant. And

$$\alpha=\eta(\dot{\gamma}^2)/k . \quad (7)$$

The boundary conditions for Eq. (6) are:

$$\begin{cases}\left[\partial T/\partial z\right]_{z=0}=0\\ \Delta T=T_{z=0.5H}-T_w=L_K\cdot\left[\partial T/\partial z\right]_{z=0.5H}\end{cases} \quad (8)$$

where L_K is the Kapitza length [16] and H is the channel height. Therefore, the temperature profile of the shear-driven flow can be predicted as:

$$T(z)=-(1/2)\alpha z^2+(1/8)\alpha H^2+T_w+(1/2)L_K\alpha H , \quad (9)$$

where T_w is wall temperature.

For the force driven flow, we also utilized the energy equation associated with the scale-affected temperature boundary conditions to calculate temperature. The combination parameter β is calculated as

$$\beta=(\rho^2g^2/\eta)/k . \quad (10)$$

Consequently, the temperature profile for force driven flow is

$$T(z)=(1/192)\beta(H^4-16z^4)+T_w+\left(1/24\right)L_K\beta H^3 . \quad (11)$$

3. Results and discussion

3.1 Density and velocity slip

In Fig. 2, the notable high-density peaks of water near solid

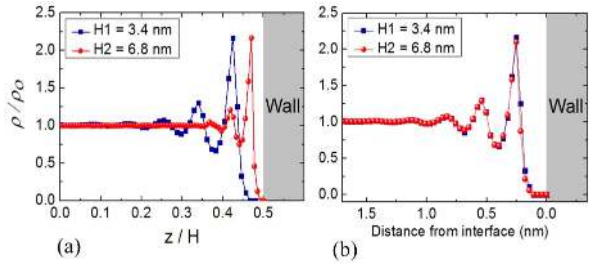

Fig. 2. Normalized density distributions of shear driven water in cases of H=3.4 nm and 6.8 nm at the same shear rate. The profiles show the view from (a) central-fluid (z=0) to the solid-liquid interface (z= 0.5 H); (b) from inner fluid to wall surface.

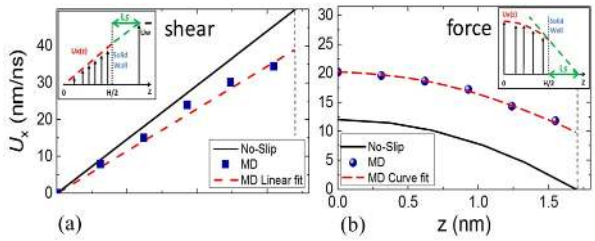

Fig. 3. Velocity distribution of the shear driven water from MD (blue-dot) and continuum no-slip prediction (black-solid line); the profiles are shown from (a) central-fluid (z=0) to solid-liquid interface (z=0.5H). (b) Velocity distribution of the force driven water with the use of similar illustration set as part (a).

surfaces show how the wall-force-penetration field affects water, illustrating the liquid layering at the solid-liquid interface. The unit sizes of the analyzed slab bin used for both models are equal. As from Fig. 2(a), the scale ratio between the interfacial density region and the bulk density region in the case of 3.4 nm H is higher than that in the case of 6.8 nm because the impact of interfacial solid molecules on water is more dominant in narrower conduits. This phenomenon differs from the behavior of thin-film water from the continuum approach. The identical interfacial-depletion-layer between the solid wall and the liquid water in Fig. 2(b) is caused by the weak Cu/water interaction strength and the solid crystal orientation [17, 18], validating the important information that the interfacial density peaks are identical under different conduit heights or other external conditions, i.e., shearing wall or driven gravity. At the central water, ρ converging to continuum water density ρ_{bulk} of 0.991 g/cm^3 theoretically satisfies the behavior of continuum fluid water and agrees with previous MD SPC/E research [9, 19].

Fig. 3(a) illustrates the slip-boundary of the shear-driven flow observed due to the nanoscale effect of the hydrophobic copper surface. Because of the weak in-plane ordering of the interfacial water, the velocity profile (Fig. 3(a)) shows a slippage of 35 m/s fluid speed near the solid surface. In the force-driven case (Fig. 3(b)), the velocity prediction using no-slip hydrodynamic concept also have different slippage with the nanoscale-simulated one. These results again illustrate the size effect of the system on the velocity slip of the flow.

Table 1. Data for assessing our results, all simulation data are for SPC/E water model at 300 K. The two first data are from our simulations. The remains are references from other researches.

Case	k (W/(K.m))	η (cP)	Refs.
SPC/E	0.680	0.714	Our work
SPC/E	-	0.710	[6]
SPC/E	-	0.670	[20]
SPC/E	0.700	-	[21]
SPC/E-modified	0.695	-	[22]
Experiment	0.609	0.798	[23]

3.2 Viscosity and thermal conductivity

Table 1 shows data for the bulk η and k of the simulated water. Our results for k and η of SPC/E water agree with other MD simulations of SPC/E water [6, 20-23]. The remarkable point is the deviation between simulation data and empirical experiment, caused by the limitation of SPC/E water in imitating η and k [21, 22]. Thermal conductivity k, as a continuum quantity, could be out of precision if being measured at a tiny scale of a few molecules [24-26]. Thus, we calculated k of the thin-film water using the Fourier's law with statistical thermodynamics concepts for the entire system. The global k of the thin-film water shows a stable value under the change of system scales or temperature gradient. Thus, k plays as the exclusively dependent property of the liquid. Our evaluated values of k in each of the 11 specified slab-bins and the whole thin-film fluid are consistently 0.680 W/K·m, which matches other published values [21-23]. Thus, k could be treated as a constant term for use in temperature predictions (Eqs. (9) and (11)).

3.3 Nanoscale Couette flow: Temperature predictions

To apply the continuum approach presented by the temperature prediction (Eq. (9)) on nanoscale water flows, it is necessary to analyze the thermodynamic properties of the fluid, such as density ρ, viscosity η, shear stress δ, shear rate $\dot{\gamma}$, and thermal conductivity k. We inferred the term of the Kapitza length (L_K) from the measured temperature jump in our MD simulation with L_K keeping constant when ($\varepsilon_{wall\text{-}O}/\varepsilon_{O\text{-}O}$) is greater or approximately equal 2 [7, 26, 27]. For ρ profiles, correcting local analysis region (slab-bins volume) lesser its deviation from the constant bulk value (Fig. 4(a)). Widening slab bin thickness (larger than water molecular diameter) [3, 12] averaged all fluctuating interfacial densities into flatter ρ. The interfacial bin is also corrected by removing the depletion space for a more accurate average ρ [5]. As shown in Fig. 4, the profiles for viscosity η, shear stress δ, and shear rate $\dot{\gamma}$ vibrate out of linear behavior because of the ambient confinements. Besides, SPC/E water is not fully optimized for the reproduction of η, and viscous-fluctuations have a peculiar effect that does not guarantee the capability of a standard averaged η [20-22]. Therefore, that fluctuation impact must be

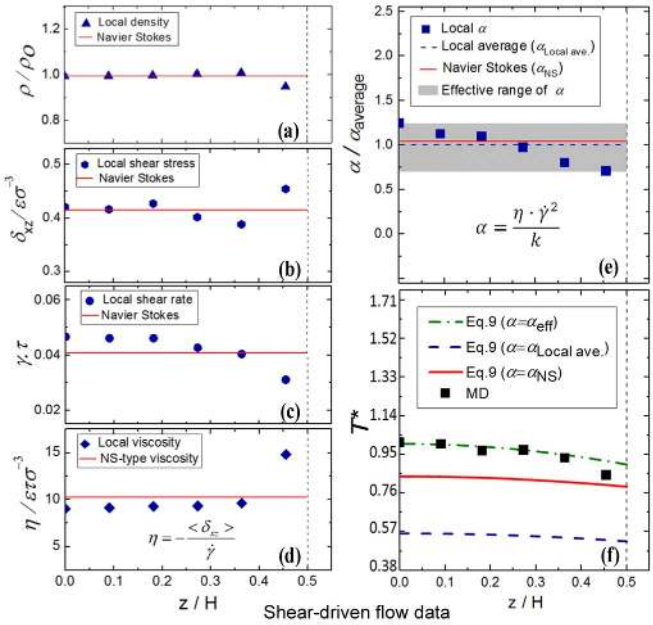

Fig. 4. (a) Distributions of density ρ; (b) shear stress δ; (c) shear rate γ; (d) viscosity η; (e) parameter α of the shear driven water with corrected-bin volume for the case of 3.6 nm channel; α_{NS} is calculated from linear-fit values. Temperature profiles (f) of the shear driven water include MD simulation (black-dot) vs. the predictions of Eq. (9) utilizing various types of α. $T^* = (T_{(z)}-T_w)/(T_H-T_w)$, where T_w is the wall temperature, T_H is highest recorded simulation temperature. $T(\alpha_{NS})$, in red, is Eq. (9) using α_{NS}. $T(\alpha_{Local\ ave.})$, in dashed blue, is Eq. (9) using $\alpha_{Local\ ave.}$; $T(\alpha_{eff})$, in dashed-dot green, is the best of Eq. (9) in predicting MD temperature by recruiting α_{eff}. The illustrating axis is from central fluid (z = 0) to solid-liquid interface (z = 0.5H). For the dimensionless unit illustrations, σ and ε are inferred from the O-O interaction when τ is the time unit of 1 picosecond.

additionally counted in Eq. (9) for this nanoscale approach. As mentioned, k is confirmed to be steady in the use of Eq. (9). The remaining factors ($\dot{\gamma}$ and η) thus strongly contribute to the prediction's accuracy due to their non-continuum behavior, inducing oscillation in α_{local} profile (Fig. 4(e)). Indeed, the viscosity of nanoconfined water has been examined to be higher than the bulk value due to liquid layering caused by surface force effect. Thus, near-surface viscosity is an important factor for temperature calculation. Early numerical experiments, i.e., Kim et al. [5] and Vo and Kim [6], found that the classical theory can describe the nanochannel flows if it takes into account the enhanced viscosity. In addition to viscosity, in this study, we considered further effects at small scale such as thermal conductivity, a density which usually differs from the bulk values. To optimize the temperature predictions by utilizing Eq. (9), we considered the inconstancy of α as a statistical averaging objective. Two methods are used to upgrading evaluate α as a constant parameter:

i: The first, "*Local average α"* ($\alpha_{\text{Local-ave.}}$), is a statistical average of the eleven local values of α from each slab-bins along z-axis distribution (Fig. 4(e)):

$$\alpha_{Local-ave.} = \left(\sum_{i=1}^{N_{bin}} \alpha_{z-bin}\right) / N_{bin}, \tag{12a}$$

where $\alpha_{z\text{-bin}}$ is α of each z-bin and N_{bin} is the number of z-bin.

ii: Inspired by upgrading continuum Navier-Stokes-type equation, the second method calculates the so-called "*Navier-Stokes-type α"* (α_{NS}) by considering α (at Eq. (6)) as the function of least-squares fitted (LSF) shear stress and LSF shear rate; i.e. (δ_{NS}) and ($\dot{\gamma}_{NS}$), respectively:

$$\alpha_{NS} = f\left(\delta_{NS}, \dot{\gamma}_{NS}, k\right). \tag{12b}$$

Because the z-profiles of this δ and $\dot{\gamma}$ treat the x-axis as the axis of symmetry at $z = 0$, their least squares-fits, therefore, are observed as constant values (z-horizontally straight lines). As a result, after being applied to Eq. (9), α_{NS} and $\alpha_{\text{Local-ave.}}$, still show the discrepancy with the simulated temperature, even though the α predictions range roughly meet the magnitude of the local α profile, i.e., the effective range of α (Figs. 4(e) and (f)). The results also show that α_{NS} is better than $\alpha_{\text{Local-ave.}}$ in matching the MD temperature profile (Fig. 4(f)).

Nonetheless, the (modified) Navier-Stokes–type predictions with α_{NS} and $\alpha_{\text{Local-ave.}}$ cannot be consistent with the MD temperature without further reconsidering the fluid properties. Indeed, because the potential of SPC/E water is not fully optimized to simulate $k_{SPC/E}$. As shown in Table 1, as well as the research of Muscatello's [22], $k_{SPC/E}$ is reportedly higher than the k of real water around 16 %, we thus need to re-correct α by correcting $k_{SPC/E}$ in use. We proposed the more-realistic k_{eff} which is smaller than our measured $k_{SPC/E}$ 16 %. Thus, we conducted the term called *the effective α* (α_{eff}) as:

$$\alpha_{eff} = \alpha_{NS} k_{SPC/E} / k_{eff}. \tag{12c}$$

The details of utilizing α_{eff} are shown in Fig. 4(f). The

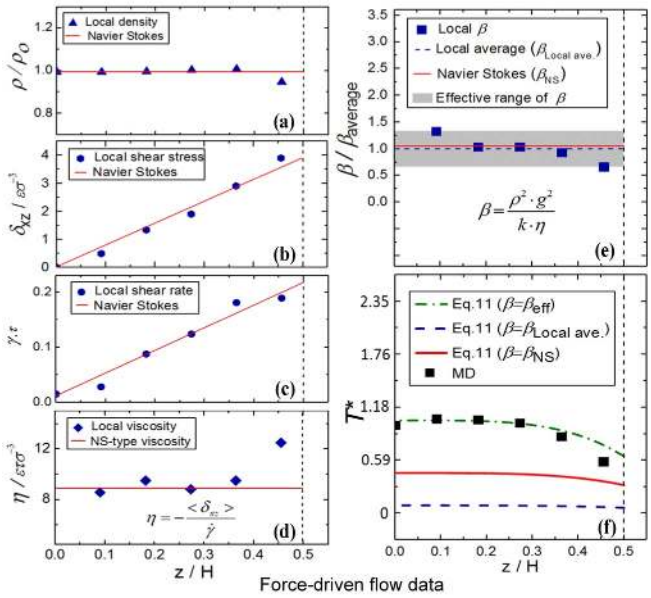

Fig. 5. (a) Distributions of density ρ; (b) shear stress δ; (c) shear rate γ; (d) viscosity η; (e) parameter β of the shear-driven water with corrected-bin volume for the case of 3.6 nm channel; β_{NS} is calculated from linear-fit values. Temperature profiles (f) of the shear driven water include MD simulation (black-dot) vs. the predictions of Eq. (11) utilizing various types of β. $T^* = (T_{(z)}-T_w)/(T_H-T_w)$; where T_w is the wall temperature, T_H is highest recorded simulation temperature. $T(\beta_{NS})$, in red, is Eq. (11) using β_{NS}. $T(\beta_{Local\ ave.})$, in dashed blue, is Eq. (11) using $\beta_{Local\ ave.}$; $T(\beta_{eff})$, in dashed-dot green, is the best of Eq. (11) in predicting MD temperature by recruiting β_{eff}. The illustrating axis is from central fluid (z = 0) to solid-liquid interface (z = 0.5H). For the dimensionless unit illustrations, σ and ϵ are inferred from the O-O interaction when τ is the time unit of 1 picosecond.

discrepancy between the central temperature of the MD profile and that of the $T(\alpha_{eff})$ profile is 0.41 K. Thus, the utilizing of α_{eff} outstandingly paid a better temperature prediction by considering the natural effects of viscous uncertainty and the overestimated simulated thermal conductivity.

3.4 Nanoscale Poiseuille flow: Temperature predictions

Because the value of the averaged β depends on the η distribution (Eq. (10)), a careful investigation is needed to observe the effective β. Similar to the explanation in Sec. 3.3, we proposed two ways of conducting the β averaging.

The first method is to average the local β values:

$$\beta_{Local-ave.} = \left(\sum_{i=1}^{N_{bin}} \beta_{z-bin}\right) / N_{bin}\,, \tag{13a}$$

where β_{z-bin} is β of each z-bin and N_{bin} is the number of z-bin.

The second method calculates the viscosity $\eta_{NS\text{-}type}$ from the ratio of the LSF shear stress (δ_{NS}) over the LSF strain rate ($\dot{\gamma}_{NS}$) along the channel height.

The result, β_{NS}, is called the *Navier-Stokes–type* β (NS-type) from upgrading Eq. (10) as:

$$\beta_{NS} = f\left(\rho_{NS}, \delta_{NS}, \dot{\gamma}_{NS}, k, g\right). \tag{13b}$$

The contribution of the Navier-Stokes-type equation (Eq. (11)) in predicting the temperature profile of the flow is shown in Figs. 5(e) and (f). From the two calculations of β above, we computed predicted temperature profiles. The averaging method using least squares-fitting following the spirit of continuum concept (Navier-Stokes type) works better than the local averaging mean. The neglected infinity values in the center fluid in Figs. 5(d) and (e), where zero shear rates induce unspecified η (Eq. (6)), could explain the poor performance of $\beta_{Local\text{-}ave.}$ (Fig. 5(e)). Even though the β prediction range roughly meets the local β (Fig. 5(e)), the predictions still show poor performance in Fig. 5(f). Thus, by considering the imperfection of $k_{SPC/E}$, we present:

$$\beta_{eff} = \beta_{NS} k_{SPC/E} / k_{eff}\,, \tag{13c}$$

as the most capable value of β to predict the fluid temperature. As shown in Fig. 5(f), the difference between the central MD-temperature and the equivalent of the effective prediction $T(\beta_{eff})$ is 0.3 K. This observation agrees with the shearing case about recruiting uncertain viscous and insufficient modeled thermal conductivity on temperature prediction of nanoscale water flow. We could see similar scenarios between our research and the work of Todd and Evans (1997) [28], that the modified temperature predictions for nanoscale fluid flow (i.e., XNS in Todd and Evans (1997), and Eq. (11) ($\beta = \beta_{eff}$) in the our work) fit the simulation results much more precisely than the conventional Navier-Stokes equations (i.e., NS in Todd and Evans (1997), and Eq. (11) ($\beta = \beta_{NS}$ or $\beta_{Local\ ave.}$) in our work). In brief, α_{eff} and β_{eff} produce better Navier-Stokes-type

temperature-predictions for the nano-water flows. The reward from this observation is that the importance of Navier-Stokes-type predictions is still available for nanoscale fluid-flow, especially water.

4. Conclusions

Due to scale effects and slippage of nano-scale water flow, reconsideration of boundary conditions and thermodynamics parameters is necessary for modified Navier-Stokes-type equations to exactly predict the fluid temperature. The $\eta_{\text{NS-type}}$ calculation combined with the linear-fit shear stress and linear-fit shear rate (NS-type) gives better temperature predictions than the local averaging method (local ave.). Moreover, by correcting $k_{\text{SPC/E}}$, in terms of α_{eff} and β_{eff}, our modified Navier-Stokes-type equation successfully predicts the fluid temperature. For quantitative assessment, we measured the relative deviation (RD) between our predictions and MD temperature. Compared to Eq. (9) (α_{NS}) or Eq. (11) (β_{NS}), by using Eq. (9) (α_{eff}) or Eq. (11) (β_{eff}) the relative deviation between MD data and prediction is reduced from 14.3 % to 2.49 % and from 51.02 % to 4.93 % for the shear-driven flow and force-driven flow, respectively. The α_{eff} and β_{eff} scientifically represent the strong effect of water slippage, viscosity, and wall penetration force on generating the inner temperature of the fluids.

Acknowledgments

This research was supported by Basic Science Research Program through the National Research Foundation of Korea (NRF) funded by the Ministry of Education (NRF-2016R1 D1A1B03932737).

Nomenclature

η	: Dynamic viscosity
k	: Thermal conductivity
δ	: Shear-stress
ρ	: Density
L_K	: Kapitza length
α	: Parameter term in T(z) prediction for sheared case
β	: Parameter term in T(z) prediction for forced case
$\dot{\gamma}$	: Shear-rate

References

[1] D. G. Cahill, W. K. Ford, K. E. Goodson, G. D. Mahan, A. Majumdar, H. J. Maris, R. Merlin and S. R. Phillpot, Nanoscale thermal transport, *J. of Applied Physics,* 93 (2003) 793-818.

[2] P. A. Thompson and S. M. Troian, A general boundary condition for liquid flow at solid surfaces, *Nature*, 389 (1997) 360-362.

[3] B. H. Kim, A. Beskok and T. Cagin, Molecular dynamics simulations of thermal resistance at the liquid-solid interface, *J. of Chemical Physics,* 129 (2008) 174701.

[4] B. H. Kim, A. Beskok and T. Cagin, Thermal interactions in nanoscale fluid flow: molecular dynamics simulations with solid-liquid interfaces, *Microfluidics and Nanofluidics,* 5 (2008) 551-559.

[5] B. H. Kim, A. Beskok and T. Cagin, Viscous heating in nanoscale shear driven liquid flows, *Microfluidics and Nanofluidics*, 9 (2010) 31-40.

[6] T. Q. Vo and B. Kim, Transport phenomena of water in molecular fluidic channels, *Scientific Reports*, 6 (2016) 33881.

[7] T. Q. Vo, B. Park, C. Park and B. Kim, Nano-scale liquid film sheared between strong wetting surfaces: Effects of interface region on the flow, *J. of Mechanical Science and Technology*, 29 (2015) 1681-1688.

[8] S. Plimpton, Fast parallel algorithms for short-range molecular dynamics, *J. of Computational Physics*, 117 (1995) 1-19.

[9] C. T. Nguyen and B. Kim, Stress and surface tension analyses of water on graphene-coated copper surfaces, *International J. of Precision Engineering and Manufacturing*, 17 (2016) 503-510.

[10] T. Q. Vo and B. Kim, Interface thermal resistance between liquid water and various metallic surfaces, *International J. of Precision Engineering and Manufacturing,* 16 (2015) 1341-1346.

[11] C. T. Nguyen and A. Beskok, Saltwater transport through pristine and positively charged graphene membranes, *J. of Chemical Physics*, 149 (2018) 024704.

[12] T. Q. Vo, M. Barisik and B. Kim, Atomic density effects on temperature characteristics and thermal transport at grain boundaries through a proper bin size selection, *J. of Chemical Physics*, 144 (2016) 194707.

[13] M. Allen and D. Tildesley, *Computer Simulation of Liquids,* Oxford Science, London (1990).

[14] C. T. Nguyen, M. Barisik and B. Kim, Wetting of chemically heterogeneous striped surfaces: Molecular dynamics simulations, *AIP Advances*, 8 (2018) 065003.

[15] M. Barisik and A. Beskok, Molecular dynamics simulations of shear-driven gas flows in nano-channels, *Microfluidics and Nanofluidics,* 11 (2011) 611-622.

[16] G. L. Pollack, Kapitza resistance, *Reviews of Modern Physics*, 41 (1969) 48.

[17] A. T. Pham, M Barisik and B Kim, Interfacial thermal resistance between the graphene-coated copper and liquid water, *International J. of Heat and Mass Transfer,* 97 (2016) 422-431.

[18] C. Y. Soong, T. H. Yen and P. Y. Tzeng, Molecular dynamics simulation of nanochannel flows with effects of wall lattice-fluid interactions, *Physical Review E*, 76 (2007).

[19] T. Q. Vo, M. Barisik and B. Kim, Near-surface viscosity effects on capillary rise of water in nanotubes, *Physical Review E*, 92 (2015) 053009.

[20] S. Nakaoka, D. Surblys, Y. Yamaguchi, K. Kuroda, T. Nakajima and H. Fujimura, Local viscosity change in the water near

a solid-liquid interface and its extraction by means of molecular rotational diffusion - A molecular dynamics study, *Chemical Physics Letters*, 591 (2014) 306-311.
[21] W. Evans, J. Fish and P. Keblinski, Thermal conductivity of ordered molecular water, *J. of Chemical Physics*, 126 (2007) 154504.
[22] J. Muscatello, F. Romer, J. Sala and F. Bresme, Water under temperature gradients: Polarization effects and microscopic mechanisms of heat transfer, *Physical Chemistry Chemical Physics*, 13 (2011) 19970-19978.
[23] B. Hess, Determining the shear viscosity of model liquids from molecular dynamics simulations, *J. of Chemical Physics*, 116 (2002) 209-217.
[24] T. Q. Vo and B. Kim, Physical origins of temperature continuity at an interface between a crystal and its melt, *J. of Chemical Physics,* 148 (2018) 034703.
[25] M. R. Hasan, T. Q. Vo and B. Kim, Manipulating thermal resistance at the solid-fluid interface through monolayer deposition, *RSC Advances,* 9 (2019) 4948-4956.
[26] B. Kim, Thermal resistance at a liquid-solid interface dependent on the ratio of thermal oscillation frequencies, *Chemical Physics Letters*, 554 (2012) 77-81.
[27] J. Sun, W. Wang and H. S. Wang, Dependence between velocity slip and temperature jump in shear flows, *J. of Chemical Physics,* 138 (2013).
[28] B. D. Todd and D. J. Evans, Temperature profile for Poiseuille flow, *Physical Review E,* 55 (1997) 2800-2807.

Quyen Van Dinh is a Ph.D. candidate in mechanical and materials engineering, Washington State University, USA. His scientific interests are molecular dynamics of micro/nano-fluidics, nanoscale biosystems, and drug delivery.

Truong Quoc Vo is a postdoctoral researcher in mechanical and process engineering, Technical University of Kaiserslautern, Germany. He received his Ph.D. in mechanical engineering from University of Ulsan, South Korea. His current scientific interests include micro-/nano-fluidics, nanoscale heat transfer, surface and interface effects and applications.

BoHung Kim is an Associate Professor of Mechanical Engineering, University of Ulsan, Korea. He received his Ph.D. in mechanical engineering from Texas A&M University, United States. His research interests are molecular neuroscience, molecular dynamics and nanoscale gas/liquid flow, and numerical method.